

A Search for H α Absorption in the Exosphere of the Transiting Extrasolar Planet HD 209458b

Joshua N. WINN^{1*}, Yasushi SUTO², Edwin L. TURNER³, Norio NARITA²,
Brenda L. FRYE^{3*}, Wako AOKI⁴, Bun’ei SATO^{4,5}, and Toru YAMADA⁴

¹*Harvard-Smithsonian Center for Astrophysics, 60 Garden St. MS-51, Cambridge, MA 02138, USA*
jwinn@cfa.harvard.edu

²*Department of Physics, School of Science, The University of Tokyo, Tokyo 113-0033*
suto, narita@utap.phys.s.u-tokyo.ac.jp

³*Princeton University Observatory, Peyton Hall, Princeton, NJ 08544, USA*
bfrye, elt@astro.princeton.edu

⁴*National Astronomical Observatory of Japan, 2-21-1, Mitaka, Tokyo 181-8588*
aoki.wako@nao.ac.jp, bunei.sato@nao.ac.jp, yamada@optik.mtk.nao.ac.jp

⁵*Graduate School of Science and Technology, Kobe University, 1-1 Rokkodai, Nada, Kobe 657-8501*

(Received 2004 April 16; accepted 2004 May 6)

Abstract

There is evidence that the transiting planet HD 209458b has a large exosphere of neutral hydrogen, based on a 15% decrement in Lyman- α flux that was observed by Vidal-Madjar et al. during transits. Here we report upper limits on H α absorption by the exosphere. The results are based on optical spectra of the parent star obtained with the Subaru High Dispersion Spectrograph. Comparison of the spectra taken inside and outside of transit reveals no exospheric H α signal greater than 0.1% within a 5.1 Å band (chosen to have the same $\Delta\lambda/\lambda$ as the 15% Ly α absorption). The corresponding limit on the column density of $n = 2$ neutral hydrogen is $N_2 \lesssim 10^9 \text{ cm}^{-2}$. This limit constrains proposed models involving a hot ($\sim 10^4$ K) and hydrodynamically escaping exosphere.

Key words: planetary systems: individual (HD 209458b)—techniques: spectroscopic

1. Introduction

A milestone in extrasolar planet research was reached when Charbonneau et al. (2000) and Henry et al. (2000) observed the photometric signal of transits by the low-mass companion of HD 209458. The companion was originally discovered by radial velocity measurements (Mazeh et al. 2000), which specified only the orbital period (3.5 days), orbital eccentricity ($e < 0.03$), and minimum mass of the companion ($M \sin i = 0.69 M_{\text{Jup}}$). The transit light curves allowed the measurement of the companion’s mass (by breaking the $\sin i$ degeneracy) and radius (from the depth of the transit), providing an unambiguous case of a planetary-mass companion to a main sequence star, and a demonstration that the companion’s density was that of a gas giant planet.

Aside from this historic importance, the discovery made possible a number of unique and important follow-up studies, based on more subtle changes in the received starlight that should occur during transits. In this paper we are concerned with changes due to the passage of a small fraction of the starlight through the planetary atmosphere. Selective absorption by atmospheric constituents causes the transit depth to depend upon wavelength, an

effect that forms the basis of “transmission spectroscopy.” Upper limits on various atmospheric absorption features have been given by Bundy and Marcy (2000), Moutou et al. (2001), Brown, Libbrecht, and Charbonneau (2002), and Moutou et al. (2003). The first successful detection using this technique was by Charbonneau et al. (2002), who observed a $(0.023 \pm 0.006)\%$ increase in transit depth in the yellow light of the sodium resonance doublet. A strong sodium signal had been predicted by Seager and Sasselov (2000), and subsequently by Brown (2001) and Hubbard et al. (2001).

More recently, Vidal-Madjar et al. (2003) reported a remarkably large transit depth of $(15 \pm 4)\%$ in the ultraviolet light of the Lyman- α (Ly α) transition of neutral hydrogen. To produce such a large absorption, a spherical cloud of neutral hydrogen would need a radius of $4.3 R_{\text{Jup}}$ or greater (depending on the optical depth), as compared to the planetary radius of $1.3 R_{\text{Jup}}$ inferred from broadband observations, and the Roche lobe radius of $3.6 R_{\text{Jup}}$. Such a signal could be produced by an extended envelope of hydrogen atoms that are evaporating from the planet’s upper atmosphere. Vidal-Madjar et al. (2003) noted that the apparent blueshift of the absorbing atoms (up to -130 km s^{-1}) provided additional evidence for atmospheric escape, and speculated that this evaporation process accounts for the rarity of extrasolar planets with orbital periods smaller than 3 days. Additional data ob-

* National Science Foundation Astronomy & Astrophysics Postdoctoral Fellow

tained by Vidal-Madjar et al. (2004) were consistent with the previous Ly α result, and provided evidence (at the 2–3 σ level) for exospheric absorption by oxygen (O I) and carbon (C II).

Further confirmation of the existence of this “exosphere,” and characterization of its temperature, density, and composition are clearly important goals. Unfortunately, theoretical predictions for the properties of the exosphere are not robust, making it difficult to design strategies for observing the exosphere. One approach is to search for additional effects of hydrogen, which has already been implicated by the Ly α measurement. If a significant fraction of the hydrogen exists in the first excited state ($n=2$), it will produce extra absorption in the Balmer lines of the stellar spectrum, and in particular H α (6563 Å).

Thus we were motivated to search for H α absorption from the exosphere of HD 209458b. A positive detection would confirm the existence of the hydrogen exosphere and constrain its density and temperature, with implications for the long-term evolution of “hot Jupiter” extrasolar planets. It would also represent a new and more practical means of searching for exospheres of other extrasolar planets, given the necessity of observing Ly α absorption above the Earth’s atmosphere, and the confusing effects of Ly α absorption by interstellar hydrogen and emission from the geocorona. Previously, Bundy and Marcy (2000) placed upper limits of 3–4% on H β and H γ absorption in a 0.3 Å band, although they did not examine H α due to contamination of that region of the spectrum by I $_2$ lines. Moutou et al. (2001) also searched for exospheric absorption in optical spectra. They did not remark on H α in particular, but set upper limits of $\approx 1\%$ for any features of width 0.2 Å, and noted that the limits could be improved significantly with higher quality spectra taken in better atmospheric conditions.

We have been obtaining optical echelle spectra of HD 209458 with the Subaru Telescope, over a wide range of planetary orbital phases, in order to search for reflected light from the planet. Data taken on the night of a planetary transit, described in section 2, are well-suited for the H α search. The procedure by which we compared the spectra taken at different times is given in section 3, and significantly improved upper limits on exospheric H α absorption are derived from the data. In section 4 we discuss the physical interpretation and provide a brief summary.

2. Observations and Data Reduction

We observed HD 209458 on UT 2002 October 25 with the Subaru 8.2 m telescope of the National Astronomical Observatory of Japan, on Mauna Kea, Hawaii. The planet was predicted to transit its parent star in the middle of that night, according to the ephemeris of Brown et al. (2001). We used the High Dispersion Spectrograph (HDS; Noguchi et al. 2002) mounted at the $f/12.5$ Optical Nasmyth focus. The entrance slit was 4'' long and 0'8 wide, oriented at a constant position angle. We used the standard Yb setup, in which the beam passes

through an order-blocking KV370 filter, is collimated by the red-optimized mirror, dispersed by the echelle grating (31.6 grooves mm $^{-1}$, blaze angle 71°25'), cross-dispersed by the red-optimized grating (250 grooves mm $^{-1}$, blaze angle 5°00'), and detected on two CCDs, each having 4100 \times 2048 pixels of size 13.5 μ m. The wavelength coverage was 4100 Å < λ < 6800 Å with resolution $R \approx 90000$.

We obtained 29 spectra of HD 209458, each with an exposure time of 500 seconds, through air masses ranging from 1.0 to 1.9. Additionally, at both the start and end of this series of exposures, we obtained a spectrum with an I $_2$ cell behind the slit (and a narrower slit width of 0'4) in order to determine accurate radial velocities for the star and verify the ephemeris. At the end of the night, we obtained 7 spectra of the B5 Vn star HD 42545 in order to estimate the telluric spectrum: any narrow absorption features in the spectrum of this rapidly rotating star ($v \sin i = 245$ km s $^{-1}$; Abt et al. 2002) are almost certainly telluric. The weather conditions were excellent, and the seeing was approximately 0'6.

We used standard IRAF¹ procedures to process the frames and extract one-dimensional spectra. The frames were debiased, trimmed, and multiplied by the gain. A median flat field was created from 20 dome-lamp exposures and normalized in two dimensions (along the dispersion, to take out the lamp spectrum, and perpendicular to the dispersion, to take out the aperture profile), and then used to correct for pixel-to-pixel sensitivity variations. A two-dimensional smooth polynomial surface was fitted to the inter-order scattered light in each frame, and subtracted. The wavelength solution was determined from thorium-argon arc exposures taken at the start and end of each night. A total of 54 orders were extracted, after fitting the trace of each order of each spectrum separately, and summing the counts across the dispersion with optimal weighting. In the order spanning H α , the pixel scale was ≈ 0.02 Å pixel $^{-1}$ and the full-width at half-maximum of arc lines was approximately 4 pixels. The resulting one-dimensional spectra had a typical signal-to-noise ratio of ≈ 300 in each pixel.

Exposures taken with the I $_2$ cell were processed separately, using the standard procedures described by Butler et al. (1996) and Sato et al. (2002). We determined the radial velocity based on the blue CCD only. Figure 1 shows our measurements, which are uncertain by ≈ 6 m s $^{-1}$, as estimated from the variance in results from 100 separate spectral segments in each exposure. The two points from October 25, obtained at the start and end of the HD 209458 observations on that night, bracket zero radial velocity (orbital phase 0.5), confirming our expectation that the transit took place between those times.

¹ The Image Reduction and Analysis Facility (IRAF) is distributed by the U.S. National Optical Astronomy Observatories, which are operated by the Association of Universities for Research in Astronomy, Inc., under cooperative agreement with the National Science Foundation.

3. Transmission Spectroscopy

During the transit, the planet blocks a portion of the stellar surface, causing the flux received from the star to decrease. Our goal was not to measure the transit light curve, which would have required observations of a comparison star to correct for flux variations due to Earth’s atmosphere. Rather, our goal was to measure differences between the light curve observed in H α and at other wavelengths, effectively using part of the parent star’s spectrum as the comparison signal. For exospheric effects to be detectable, they must not only be large enough to overcome the Poisson noise in the starlight, but they must also be distinguished from spectral variations caused by instabilities in the Earth’s atmosphere and the spectrograph. In this section we describe the method we used to attempt to make this distinction.

3.1. Corrections for Instrumental Variations

Figure 2 compares two representative spectra that were taken 2.5 hours apart. The top three panels show three consecutive orders bracketing H α , the strong absorption feature at 6563 Å. We refer to these spectra as $S_1(\lambda_{n,j})$ and $S_2(\lambda_{n,j})$, where $\lambda_{n,j}$ is the j th wavelength bin within the n th spectral order. Note that we have not normalized the spectra; the continua are peaked near the middle of each order due to the blaze function of the spectrograph.

The green points in the bottom three panels of figure 2 show the ratios $R(\lambda_{n,j}) = S_1(\lambda_{n,j})/S_2(\lambda_{n,j})$. The mean of the ratio spectrum is not unity, which is expected, because of variations in total flux received in each exposure caused by the Earth’s atmosphere. More surprising are the wavelength variations in the ratio spectra: there are $\pm 5\%$ variations varying smoothly over ≈ 5 Å scales. We believe these variations are not an artifact of the extraction procedure, because the same variations were obtained from spectra that were extracted using different aperture sizes, and from spectra that were extracted using custom-built procedures in the Interactive Data Language (IDL) rather than IRAF.

The variations are surely instrumental, because the pattern is very similar in each order: the ratio spectrum is a function of j rather than λ , and depends on n to a much lesser degree. The ratio spectra also exhibit a smooth time dependence. In particular, the wavelength variations are greatest when one of the spectra involved in the ratio was taken at the beginning of the night. This was when the target was near zenith and the instrument rotator was moving most quickly. The ratio spectra are flatter when the two spectra were taken with nearly the same rotation angle. For these reasons, we hypothesize that these apparent variations in the blaze function are caused by flexure of the spectrograph. Similar variations have been seen by other observers using Subaru/HDS (e.g., Nagao et al. 2003) and also Keck/HIRES (e.g., Suzuki et al. 2003).

We corrected for this effect empirically by using the pattern observed in the adjacent orders. To correct the n th order, we computed $R(\lambda_{n+1,j})$ and $R(\lambda_{n-1,j})$, and then smoothed each of these functions in j with a boxcar size

of 100 pixels (2 Å), giving $\tilde{R}(n+1,j)$ and $\tilde{R}(n-1,j)$. We then used linear regression to determine the two numbers c_{n+1} and c_{n-1} that minimized the sum of squared residuals between S_1 and

$$S_{2b}(\lambda_{n,j}) = [c_{n+1}\tilde{R}(n+1,j) + c_{n-1}\tilde{R}(n-1,j)]S_2(\lambda_{n,j}). \quad (1)$$

For a given pair of spectra we typically found $c_{n+1} \approx c_{n-1} \approx 0.5$. The resulting “blaze corrected” ratio spectrum, S_1/S_{2b} , is near unity with a standard deviation within 10% of that expected from the Poisson statistics (see black dots in figure 2).

Next, we corrected for small variations in the wavelength scale by determining the two numbers c_0 and $\Delta\lambda$ that provided the best match between S_1 and

$$S_{2m}(\lambda_{n,j}) = c_0 S_{2b}(\lambda_{n,j}) + \Delta\lambda \frac{dS_{2b}(\lambda)}{d\lambda}, \quad (2)$$

where the derivative was approximated numerically by 3-point Lagrangian interpolation. The wavelength shifts were always smaller than 0.005 Å (0.25 pixel). We refer to S_{2m} as the “matched” spectrum; it has been matched in blaze function and wavelength scale to S_1 .

3.2. Calculation of Difference Spectra

Having established this matching procedure to correct for instrumental variations between any pair of spectra, we created a template spectrum with a high signal-to-noise ratio in the following manner. A spectrum from the middle of the night was chosen as a reference spectrum. All the spectra taken through an air mass less than 1.4 were matched to the reference spectrum. (Spectra taken through larger air masses were significantly contaminated by time-variable telluric lines, as will be seen shortly.) The preliminary template spectrum was defined as the median of all the matched spectra. Then, the entire procedure was repeated, using the preliminary template spectrum as the reference spectrum, resulting in the final template spectrum $T(\lambda)$. Finally, a time series of difference spectra was created, by subtracting each spectrum from the suitably matched template.

Some examples of the difference spectra are shown in figure 3, for a 55 Å region in the vicinity of H α . The difference spectra are plotted in units of Poisson deviates,

$$\frac{S(\lambda) - T_m(\lambda)}{\sqrt{T_m(\lambda)}}, \quad (3)$$

with the space between minor tick marks indicating one Poisson deviation. Also plotted are the template spectrum (bottom) and the estimated telluric spectrum (top). To produce the telluric spectrum, we created a template spectrum for HD 42545 in the same way as we did for HD 209458. Then we removed the rotationally broadened H α absorption line (which had a full-width at half-maximum of ~ 11 Å) by fitting a smooth polynomial to the spectrum and dividing by this polynomial. We note that the telluric spectrum is shown for visual reference only; we did not use it in any of the calculations described below.

The difference spectra are nearly consistent with Poisson noise: they have standard deviations near unity,

as expected. However, a close inspection of figure 3 shows the residuals are not truly random. For spectra taken through large air masses (late times), telluric lines are visible. In addition, there are excursions of order $1-2\sigma$ that are evident as “ripples” on scales of $2-5 \text{ \AA}$ (100–250 pixels). For example, the spectrum at $t = 0.24$ shows a sawtooth pattern in the residuals between 6535 and 6545 \AA . We do not know the cause of these ripples, but we are confident that they are not due to the exosphere of the planet, for two reasons: they are not specific to any particular absorption line in the stellar spectrum; and they also appear in spectra taken on October 27, when the planet was not transiting.

3.3. Calculation of Difference Light Curves

There are no obviously significant features in the difference spectra at the position of $\text{H}\alpha$, implying that once the spectra have been adjusted to correct for total flux and instrumental effects, there is no significant difference between the $\text{H}\alpha$ light curve and those of neighboring bands. To plot these light curves, we computed the fractional difference in flux between the spectrum and the matched template,

$$\delta(t) = \frac{\int_{\lambda_1}^{\lambda_2} d\lambda [S(\lambda, t) - T_m(\lambda)]}{\int_{\lambda_1}^{\lambda_2} d\lambda T_m(\lambda)} \quad (4)$$

for the 3 different wavelength bands indicated in figure 3: a band centered on $\text{H}\alpha$ (green), and two comparison bands (red and blue) in the adjacent continua. The width of the $\text{H}\alpha$ band (5.13 \AA) was chosen to match the $\Delta\lambda/\lambda$ of the band over which Vidal-Madjar et al. (2003) reported $\text{Ly}\alpha$ absorption. The central wavelength of the $\text{H}\alpha$ band was shifted to compensate for the time-variable Doppler shift of the planetary orbit. This shift is evident as a tilt in the green lines of Figure 3. The central wavelengths of the comparison bands were chosen to avoid telluric lines and strong stellar absorption lines, as much as possible. The widths of the red (3.87 \AA) and blue (3.61 \AA) comparison bands were chosen such that all three bands have the same total flux in the template spectrum. Figure 4 shows the light curve $\delta(t)$ for each of the three bands. Apart from a few outliers, the variations in the $\text{H}\alpha$ band are similar in size and character to the variations in the comparison bands. The red and blue light curves exhibit small (and opposite) gradients which are probably effects of increasing air mass.

To place a quantitative limit on excess $\text{H}\alpha$ absorption, we calculated $\bar{\delta}_{\text{in}}$, the mean value of $\delta(t)$ for spectra taken during transit (between second and third contacts). As an estimate of the uncertainty in $\bar{\delta}_{\text{in}}$, we computed the standard deviation of $\delta(t)$ for the 12 in-transit spectra and divided by $\sqrt{12}$. Likewise, we computed $\bar{\delta}_{\text{out}}$ and its uncertainty from the spectra taken before first contact or after fourth contact.² Then we computed $\delta_{\text{H}\alpha} \equiv \bar{\delta}_{\text{in}} - \bar{\delta}_{\text{out}}$, which would be negative if there were extra $\text{H}\alpha$ absorption

during transit. For the 5.13 \AA band, the result is $\delta_{\text{H}\alpha} = -0.00024 \pm 0.00029$. We investigated the dependence of this limit upon bandwidth, by repeating this procedure for bands varying in width from 0.5 \AA to 10 \AA , centered on $\text{H}\alpha$. The results are shown in the upper right panel of figure 4. Finally, we tried blueshifting the 5.13 \AA $\text{H}\alpha$ band by -130 km s^{-1} , to match the possible blueshift in $\text{Ly}\alpha$ observed by Vidal-Madjar et al. (2003). The outcome was also a null result, $\delta_{\text{H}\alpha} = 0.00015 \pm 0.00021$.

Although our spectrum-matching procedure was intended to correct only for instrumental and telluric effects, it also acts to dilute any real signal. To estimate the size of this effect we injected an artificial signal into the data. We multiplied the extracted spectra by $(1 - g_\lambda)$, where g_λ is a Gaussian function centered on $\text{H}\alpha$ with a full-width at half-maximum of 3 \AA (a fairly arbitrary choice, since the true width of the absorbing feature is unknown), representing a total flux decrement of 0.1% in the 5.13 \AA band over which $\delta_{\text{H}\alpha}$ was measured. When the preceding analysis was performed on the adulterated data, the result was $\delta_{\text{H}\alpha} = -0.00081 \pm 0.00028$. This is greater by 0.00057 than the measurement with no artificial signal, verifying that the artificial signal (although diluted) could be recovered in spite of the noise. We conclude that an extra 0.1% absorption during transit would have been detected. Figure 5 shows the resulting light curve $\delta(t)$ and the “measured” absorption as a function of the width of the $\text{H}\alpha$ band.

4. Discussion and summary

Fundamentally, our null result corresponds to a maximum number of neutral hydrogen atoms in the $n = 2$ state that are present in the exosphere of HD 209458b. Likewise, the detection of $\text{Ly}\alpha$ absorption by Vidal-Madjar et al. (2003) implies a minimum number of neutral hydrogen atoms in the $n = 1$ state. Unfortunately it is difficult to use these results to constrain interesting quantities such as the exospheric temperature and density, because the physical conditions in the exosphere are likely to be quite complex. The column density of neutral hydrogen may vary widely across the surface of the primary star due to evaporation, tidal forces, and radiation pressure (see, e.g., Lecavelier des Etangs et al. 2004). Gas may be present at a variety of temperatures and densities, and may be far from local thermodynamic equilibrium (LTE). [Even in the denser atmosphere, non-LTE effects may be required to explain the unexpectedly weak detection of sodium by Charbonneau et al. (2002), as proposed by Barman et al. (2002) and Fortney et al. (2003).] Obviously the limited empirical information available is not sufficient by itself to determine a realistic physical exosphere models.

With these caveats, we can use a simple order-of-magnitude argument to provide an upper limit on the column density of $n = 2$ neutral hydrogen that exosphere

J.D. (mid-transit) = 2451659.93675 (Brown et al. 2001) and the most precise published period, $P = 3.524739 \text{ d}$ (Robichon and Arenou 2000).

² To compute the transit times, we used an ephemeris defined by

models will need to obey. In order to translate our upper limit on additional H α absorption into a corresponding upper limit on the H α equivalent width, we combined the in-transit spectra to form $S_{\text{in}}(\lambda)$, and we combined the out-of-transit spectra to form $S_{\text{out}}(\lambda)$. Then the equivalent width W_λ of any transit absorption feature is

$$W_\lambda \approx \int d\lambda \left[\frac{S_{\text{out}}(\lambda) - S_{\text{in}}(\lambda)}{S_{\text{out}}(\lambda)} \right]. \quad (5)$$

Performing the integral over the 5 Å band described in the previous section, we find $W_{\text{H}\alpha} < 1.7$ mÅ. If we further assume that the fraction of the stellar surface covered by the exosphere is $\Delta A/A \approx 0.15$ (as estimated from the Ly α result), then the null result implies that H α absorption is weak, and the corresponding limit on the column density of $n = 2$ atoms (N_2) is determined via

$$\left(\frac{\Delta A}{A} \right) W_{\text{H}\alpha} = \frac{\pi e^2}{mc^2} f_{23} \lambda_{\text{H}\alpha}^2 N_2, \quad (6)$$

where $f_{23} \approx 0.641$ is the oscillator strength of the $n = 2 \rightarrow 3$ transition. The resulting limit is $N_2 < 1.0 \times 10^9 \text{ cm}^{-2}$.

In principle, N_1 could be estimated from the Ly α decrement observed during transits, and the ratio N_2/N_1 could be related to the H I excitation temperature. In reality, N_1 is highly uncertain because the absorption is probably saturated, and the line profile is unobservable due to interstellar absorption and geocoronal emission. However, any exosphere model that specifies N_1 is constrained by our results to have a maximum excitation temperature T_{ex} , according to the relation

$$\frac{N_2}{N_1} = \frac{g_2}{g_1} \exp\left(-\frac{E_2 - E_1}{kT_{\text{ex}}}\right) = 4 \exp\left(-\frac{10.2 \text{ eV}}{kT_{\text{ex}}}\right). \quad (7)$$

This constraint appears to be important in the context of recently proposed models in which the exosphere is very hot and hydrodynamically escaping, as argued below.

The temperature of the lower atmosphere of HD 209458b is likely to be near the radiative effective temperature, $T_{\text{eff}} \approx 10^3$ K, at which the $n = 2$ population predicted from equation (7) is utterly negligible. But, as argued by Moutou et al. (2001), Lammer et al. (2003), and Lecavelier des Etangs et al. (2004), the exosphere is likely to be significantly hotter than T_{eff} , just as the exosphere of Jupiter is considerably hotter than its lower atmosphere ($\sim 10^3$ K vs. 150 K; see, e.g., Atreya 1986). Lammer et al. (2003) found that close-in gas giant planets could have exospheric temperatures up to 10^4 K due to intense X-ray and extreme-ultraviolet (EUV) irradiation. Depending on the density of neutral hydrogen and other factors, such a hot exosphere could produce detectable H α absorption in violation of our constraint.

For example, Lecavelier des Etangs et al. (2004) presented 3 models for the thermosphere and exosphere of HD 209458b. In each case they specified the density profile of neutral hydrogen and computed the size and shape of the exosphere as a function of kinetic temperature T_k , taking tidal distortion into account. For the specific case of Model A, the density is $n_{\text{HI}} = 2 \times 10^9 \text{ cm}^{-3}$ at the

base of the thermosphere, and decreases with radius according to the barometric law. We computed the average column density N_1 within the annulus reaching from the thermobase to the Roche radius, and then used equation (7) to translate our upper limit on N_2 into an upper limit on the excitation temperature, finding $T_{\text{ex}} < 8000$ K. By comparison, Lecavelier des Etangs et al. (2004) found that $T_k > 8000$ K in order to produce an escape rate of 10^{10} g s^{-1} [the lower limit inferred by Vidal-Madjar et al. (2003)], and $T_k > 11100$ K through a simulation of EUV heating. Of course, one would not necessarily expect $T_{\text{ex}} \approx T_k$ in the tenuous thermosphere and exosphere, because of departures from LTE; in general, T_{ex} is neither an upper bound nor a lower bound on T_k . The $n = 2$ state may be depopulated when collisions are infrequent, and likewise, whatever process accelerates the gas to $\sim 100 \text{ km s}^{-1}$ may overpopulate the $n = 2$ state via recombination cascades and Ly α resonant trapping. A full non-LTE exosphere model will need to accommodate the resulting upper limit on the excitation temperature.

In summary, we have used high resolution and high signal-to-noise ratio Subaru-HDS optical spectra to search for excess Balmer H α absorption during a transit of the extrasolar planet HD 209458b. No excess absorption was detected. Our upper limit is two orders of magnitude below the Ly α absorption reported by Vidal-Madjar et al. (2003, 2004). It may be difficult to improve upon this limit with ground-based instruments, given the difficulty of correcting for telluric and instrumental spectral variations. However, there should be no obstacle to improving upon our limit with space-based spectroscopy, and we are aware that such an effort is underway using data from the Hubble Space Telescope (Charbonneau, D., private communication). The current result, and any future refinements, will be useful in the further development of models for the escape of the hot exospheres of close-in gas giant planets.

We are very grateful to Yutaka Abe, Dave Charbonneau, Bruce Draine, Bob Kurucz, Avi Loeb, Paul Martini, Dimitar Sasselov, and Motohide Tamura, for helpful consultations. This work is based on data from the Subaru Telescope, which is operated by the National Astronomical Observatory of Japan. We wish to recognize and acknowledge the very significant cultural role and reverence that the summit of Mauna Kea has always had within the indigenous Hawaiian community. We are most fortunate to have the opportunity to conduct observations from this mountain.

References

- Abt, H.A., Levato, H., & Grosso, M. 2002, *ApJ*, 573, 359
- Atreya, S. K. 1986, *Atmospheres and ionospheres of the outer planets and their satellites*, Springer Series on Physics and Chemistry in Space, Volume 15, (Springer-Verlag: Berlin and New York), 31
- Barman, T. S., Hauschildt, P. H., Schweitzer, A., Stancil, P. C., Baron, E., & Allard, F. 2002, *ApJL*, 569, L51

- Brown, T. M. 2001, *ApJ*, 553, 1006
- Brown, T. M., Charbonneau, D., Gilliland, R. L., Noyes, R. W., & Burrows, A. 2001, *ApJ*, 552, 699
- Brown, T. M., Libbrecht, K. G., & Charbonneau, D. 2002, *PASP*, 114, 826
- Bundy, K.A., & Marcy, G.W. 2000, *PASP*, 112, 1421
- Butler, R.P., Marcy, G.W., Williams, E., McCarthy, C., Dosanji, P., & Vogt, S.S. 1996, *PASP*, 108, 500
- Charbonneau, D., Brown, T. M., Latham, D. W., & Mayor, M. 2000, *ApJ*, 529, L45
- Charbonneau, D., Brown, T. M., Noyes, R. W., & Gilliland, R. L. 2002, *ApJ*, 568, 377
- Fortney, J. J., Sudarsky, D., Hubeny, I., Cooper, C. S., Hubbard, W. B., Burrows, A., & Lunine, J. I. 2003, *ApJ*, 589, 615
- Henry, G. W., Marcy, G. W., Butler, R. P., & Vogt, S. S. 2000, *ApJ*, 529, L41
- Hubbard, W. B., Fortney, J. J., Lunine, J. I., Burrows, A., Sudarsky, D., & Pinto, P. 2001, *ApJ*, 560, 413
- Lammer, H., Selsis, F., Ribas, I., Guinan, E. F., Bauer, S. J., & Weiss, W. W. 2003, *ApJ*, 598, L121
- Lecavelier des Etangs, A., Vidal-Madjar, A., McConnell, J. C., & Hébrard, G. 2004, *A&A*, 418, L1
- Mazeh, T., et al. 2000, *ApJ*, 532, L55
- Moutou, C., Coustenis, A., Schneider, J., St Gilles, R., Mayor, M., Queloz, D., & Kaufer, A. 2001, *A&A*, 371, 260
- Moutou, C., Coustenis, A., Schneider, J., Queloz, D., & Mayor, M. 2003, *A&A*, 405, 341
- Nagao, T., Murayama, T., Shioya, Y., & Taniguchi, Y. 2003, *AJ*, 126, 1167
- Naef, D., Mayor, M., Beuzit, J.L., Perrier, C., Queloz, D., Sivan, J.P., & Udry, S. 2004, *A&A*, 414, 351
- Noguchi, K., et al. 2002, *PASJ*, 54, 855
- Robichon, N., & Arenou, F. 2000, *A&A*, 355, 295
- Sato, B., Kambe, E., Takeda, Y., Izumiura, H., & Ando, H. 2002, *PASJ*, 54, 873
- Seager, S., & Sasselov, D.D. 2000, *ApJ*, 537, 916
- Suzuki, N., Tytler, D., Kirkman, D., O'Meara, J. M., & Lubin, D. 2003, *PASP*, 115, 1050
- Vidal-Madjar, A., Lecavelier des Etangs, A., Désert, J.-M., Ballester, G.E., Ferlet, R., Hébrard, G., & Mayor, M. 2003, *Nature*, 422, 143
- Vidal-Madjar, A., et al. 2004, *ApJ*, 604, L69

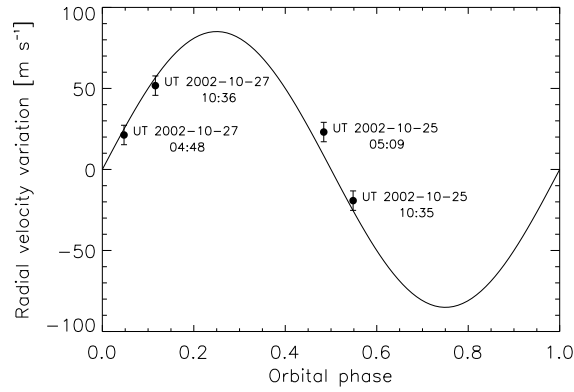


Fig. 1. Subaru radial velocity measurements of HD 209458 on 2002 October 25 and 27. The full radial velocity curve is also plotted, using the orbital parameters determined by Naef et al. (2004). This confirms that the planetary transit took place between the times of our two measurements on October 25, which bracketed the time series of spectra presented in this paper.

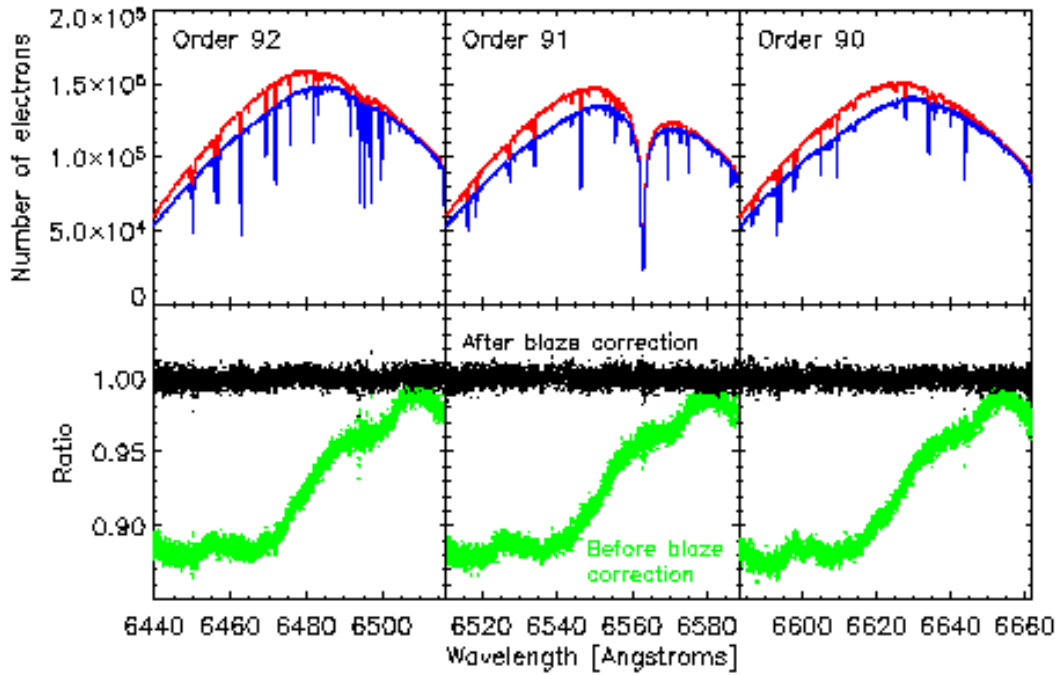


Fig. 2. The top panels show sample spectra of HD 209458 taken 2.5 hours apart. Each panel shows one order. The bottom panels show the ratio of the spectra, both before (green) and after (black) the blaze function correction.

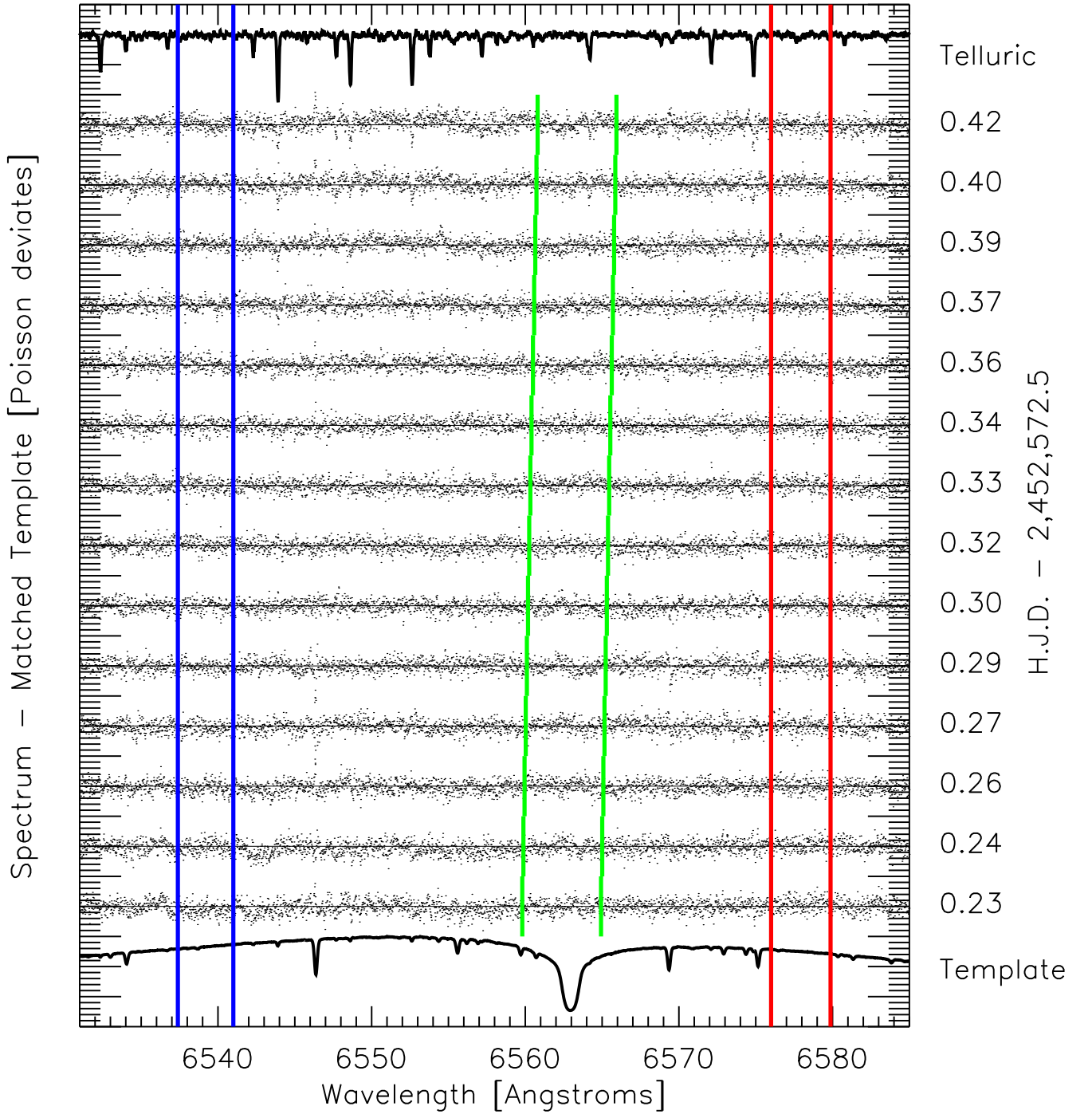


Fig. 3. Differences between individual spectra of HD 209458 and the matched template, expressed in units of Poisson deviates. The spacing between minor tick marks represents one Poisson deviation. For clarity, only 14 of the 29 spectra are shown. The template spectrum is depicted at the bottom of the series, and the telluric spectrum is depicted at the top. The right-hand axis shows the time each spectrum was taken, in the same units as figure 4. Colored lines mark the edges of the three band passes described in the text.

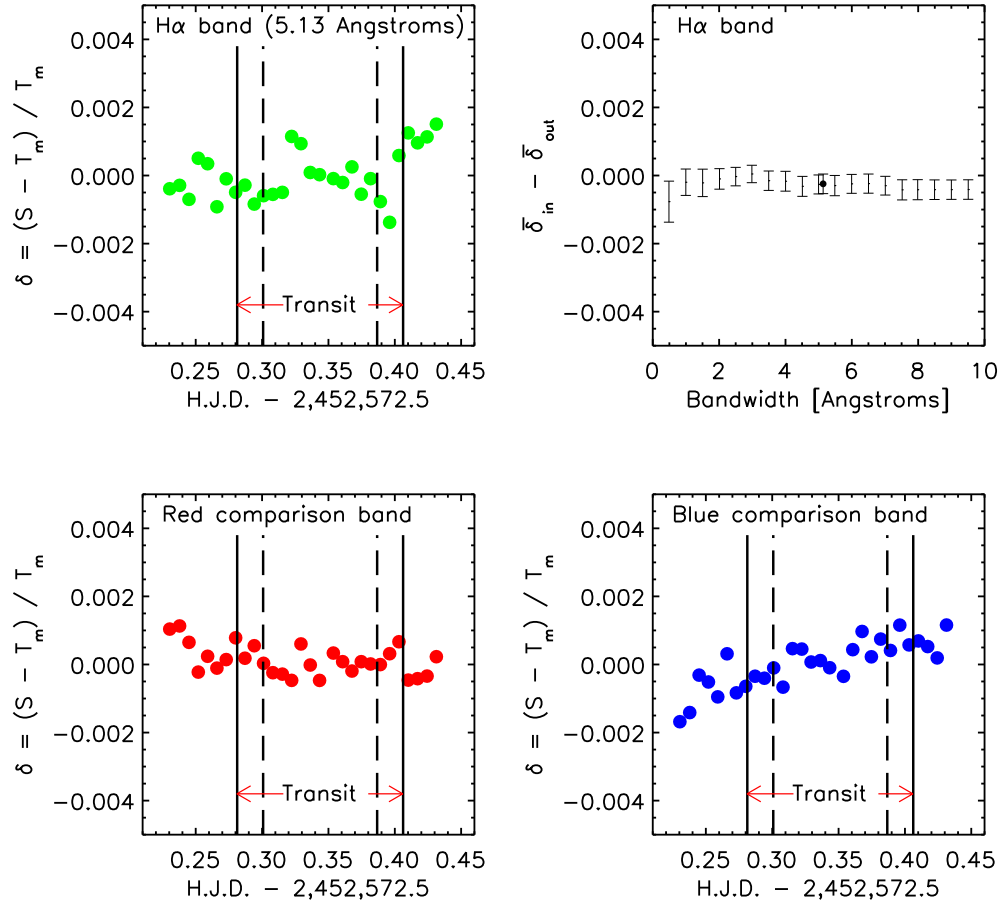


Fig. 4. Comparison of the H α light curve and light curves in adjacent bands. (Top left) The fractional difference in flux between each spectrum S and the corresponding matched template T_m , within the 5.1 Å H α band shown in figure 2. Solid lines indicate the times of first and fourth contact. Dashed lines indicate the times of second and third contact. (Bottom left) Same, but for the red comparison band. (Bottom right) Same, but for the blue comparison band. (Upper right) The difference between in-transit and out-of-transit flux deviations from the template, as a function of the width of the band pass. The single filled point is for the 5.1 Å band.

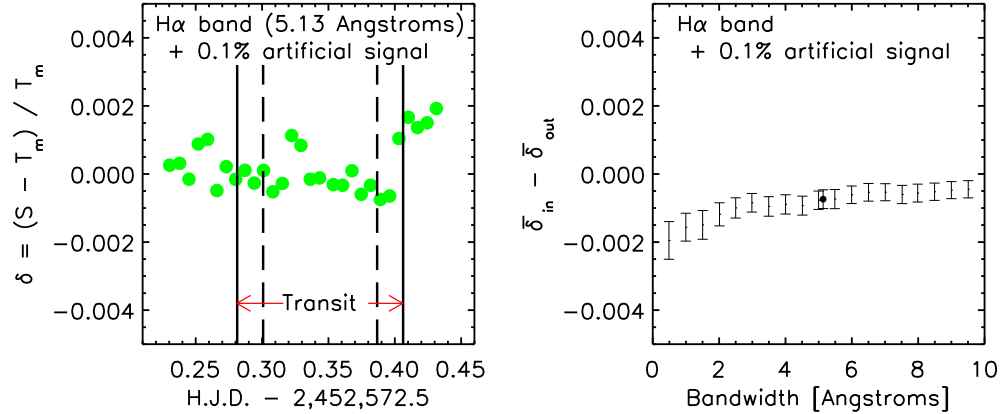


Fig. 5. Same as the top two panels of figure 4, except that an artificial absorption signal of strength 0.1% has been added to the in-transit spectra. From this test we concluded that a 0.1% excess in H α absorption during transits would have been detected.